Collective spin modes in chains of dipolarly interacting rectangular magnetic dots

R. Zivieri,[1] F. Montoncello,[1] L. Giovannini,[1] F. Nizzoli,[1] S. Tacchi,[2] M. Madami,[2] G. Gubbiotti,[2,3] G. Carlotti,[2,4] and A. O. Adeyeye[5]

[1]*CNISM Unità di Ferrara, Dipartimento di Fisica, Università di Ferrara, Via Saragat 1, I-44121 Ferrara, Italy*

[2]*CNISM Unità di Perugia, Dipartimento di Fisica, Università di Perugia, Via Pascoli, I-06123 Perugia, Italy*

[3]*Istituto Officina dei Materiali del CNR (CNR-IOM), Unità di Perugia, c/o Dipartimento di Fisica, Via A. Pascoli, I-06123 Perugia, Italy*

[4]*Centro S3, CNR-Istituto di Nanoscienze, Via Campi 213A, I-41125 Modena, Italy*

[5]*Information Storage Materials Laboratory, Department of Electrical and Computer Engineering, National University of Singapore, Singapore 117576*

(Received 27 July 2010; revised manuscript received 10 November 2010; published 24 February 2011)

We present a combined experimental and micromagnetic study of spin excitations in chains of dense magnetic dots. The samples consist of long chains of rectangular dots with rounded corners having lateral dimensions of 715×450 nm^2 and 1025×450 nm^2, respectively. Chains are composed of magnetic elements put side by side along either their major or minor axis with edge-to-edge separation below 100 nm. The frequency dispersion of the spin-wave excitations was measured by Brillouin light-scattering technique as a function of the transferred wave vector directed along the chains of dots and for an external magnetic field applied perpendicularly to the transferred wave vector in the dots plane. Evidence is given of collective excitations in the form of Bloch waves propagating through the chains characterized by magnonic energy bands. Micromagnetic calculations, performed by using the dynamical matrix method, enable us to satisfactorily reproduce the frequency dispersion of collective spin modes as well as to visualize the spatial profile of the dynamic magnetization inside the dots. We also propose a general rule to understand the frequency dispersion of collective modes starting from the relative phase of dynamic magnetization in the facing sides of adjacent dots.

DOI: 10.1103/PhysRevB.83.054431 PACS number(s): 75.30.Ds, 78.35.+c, 75.78.Cd

I. INTRODUCTION

In this last decade the study of magnetization dynamics in magnetic nanostructures has received great attention both from theoreticians and experimentalists. Very interesting properties associated to the laterally confined nanostructures were found in the spin-wave spectrum, such as the "nondispersive" behavior of spin-wave modes in magnetic elements of different shapes and of different materials.[1,2] When elements form a closely packed array, the standing waves of individual elements can interact via dynamic dipolar magnetic coupling and form collective spin excitations which do show dispersive behavior and can be assumed to be Bloch-type modes.[3] This is due to the dynamic dipolar magnetic field which removes the degeneracy between discrete energy levels of different magnetic elements. In analogy to the well established field of photonic crystals in optics, these magnetic systems constitute a new class of artificial crystals, now known as magnonic crystals, in which collective spin excitations rather than light are used to transmit and process information.[4–9] A deep comprehension of the role played by dynamic coupling is highly desirable and may be very useful to understand the speed limits of new magnetic logic gates in the GHz frequency range and new microwave devices. New schemes for building logic gates by combining chains of finite length or clusters in a quasi-two-dimensional structure where magnetic dots are designed to behave as compasses have been proposed in the literature.[10] Because of the small lateral dimensions, dots were in a single domain state and their magnetization orientation was changed in a dominolike cascade whereby the orientation of the magnetization propagates along a line or inside a cluster of dots coupled by magnetic stray field between elements. In such logical schemes, exploiting dipole coupling of the dots, excitation of collective spin-wave modes is inevitable. Spurious dynamic dipole coupling of adjacent elements will limit the minimum distances between them and thus determine the maximum density of elements per unit area. In addition to this, any magnetic logic competition with traditional semiconductor-based logic must be able to operate at GHz rates or better in the THz range.

In previous works it was shown that chains of closely packed one-dimensional (1D) magnetic nanostripes support propagation of collective magnetic eigenexcitations whose frequencies lie in the GHz range[7,11–13] with Brillouin-zone boundaries determined by the artificial periodicity of the arrays. The aim of the present work is to determine the collective dynamic properties of chains of dots and to see how the two-dimensional (2D) lateral confinement of magnetic elements modifies the dispersion law and the mode's nature with respect to the 1D case of stripes. Calculations have been performed by using the dynamical matrix method (DMM),[14] which has proven to give insight into the spin dynamics in arrays of noninteracting dots, mode localization and splitting, and magnetization reversal.[15] In this work we used the modified version of the DMM which has been extended to the case of interacting dots with spin-wave modes in the Bloch form.[16]

Such chains of rectangular magnetic elements can be considered as an example of a 1D waveguide, in analogy to the nanostripe with periodic width modulation proposed by Lee *et al.*[17] In Ref. 17 the allowed and forbidden bands were predicted for propagating dipole-exchange spin waves that appeared as the result of a relatively weak Bragg backscattering at the edge steps of the width-modulated nanostripe.

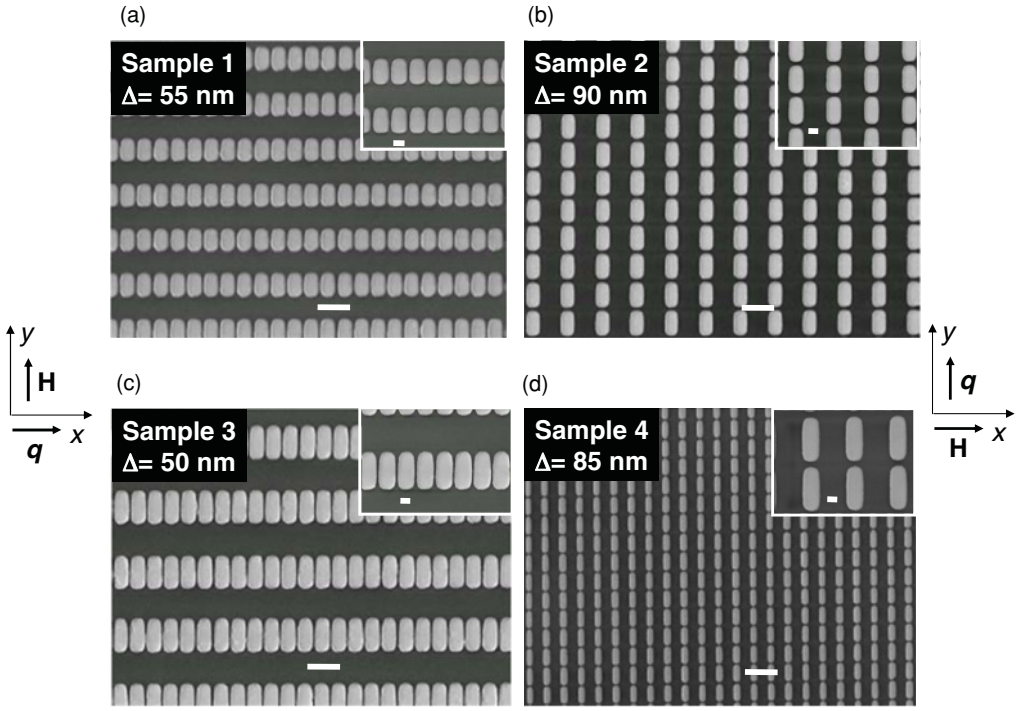

FIG. 1. SEM images of the four studied systems. (a) Sample 1, rectangular dots with lateral dimensions 715×450 nm^2 put side by side along the major axis. (b) Sample 2, rectangular dots with lateral dimensions 715×450 nm^2 put side by side along the minor axis. (c) Sample 3, as in panel (a), but with dots of lateral dimensions 1025×450 nm^2. (d) Sample 4, as in (b), but with dots of lateral dimensions 1025×450 nm^2. The in-plane axes of the reference frame and the directions of the exchanged wave vector $\boldsymbol{q}$ and external magnetic field $\mathbf{H}$ are shown. A field of magnitude $H = 1$ kOe was applied along the y axis for dispersion shown in (a) and (c). A field of magnitude $H = 1.5$ kOe was applied along the x axis for dispersion shown in (b) and (d). The wave vector $\boldsymbol{q}$ was along the chains (either along the x axis or y axis). The white scale bars represent 1 μm in the micrographs and 200 nm in the insets.

These predictions have been recently confirmed by a micro-focused Brillouin light-scattering study on a microstructured waveguide where the thickness of the stripe was increased with respect to the original theoretical work to improve the spin-wave group velocity. As a consequence of the spin-wave reflection caused by the periodical waveguide width and the modulation of the internal magnetic field, rejection frequency band was observed and its frequency position was tuned by the dc bias field.[18] In our case, the physical mechanisms giving rise to collective-mode formation is different in the sense that one starts from a set of discrete frequencies (corresponding to individual resonances inside each rectangular element) whose degeneracy is removed by dynamic dipolar magnetic coupling acting as a relatively weak perturbation of the individual resonances.

II. SAMPLE PREPARATION AND EXPERIMENTAL SETUP

Periodic arrays of $Ni_{80}Fe_{20}$ chains of rectangular elements 40 nm thick were fabricated on commercially available silicon substrate using deep ultraviolet lithography at 248 nm exposing wavelength followed by the lift-off process. To create patterns in the resist, the substrate was coated with a 60-nm-thick antireflective layer followed by a 480-nm positive deep ultraviolet photoresist. A Nikon lithographic scanner with KrF excimer laser radiation was used to expose the resist. To convert the resist patterns into dots 40 nm thick, $Ni_{80}Fe_{20}$ was deposited using e-beam evaporation at a rate of 0.2 Å/s. The pressure was maintained at 2×10^{-6} Torr during deposition. Lift-off of the deposited film was carried out in isopropyl alcohol. Completion of the lift-off process was determined by the color contrast of the patterned $Ni_{80}Fe_{20}$ area. The rectangular elements have lateral dimensions of 715×450 nm^2 and 1025×450 nm^2 and are arranged in two different configurations. In Fig. 1 the scanning electron microscopy (SEM) images of the four samples studied are shown.

Sample 1: chains of dots having lateral dimensions of 715×450 nm^2 placed side by side along the major axis with an edge-to-edge distance $\Delta = 55$ nm [periodicity $a = 505$ nm, first Brillouin-zone (1BZ) boundary $q_{BZ} = \pi/a = 0.62 \times 10^5$ rad/cm].

Sample 2: chains of dots having lateral dimensions of 715×450 nm^2 placed side by side along the minor axis with an edge-to-edge distance $\Delta = 90$ nm (periodicity $a = 805$ nm, 1BZ boundary $q_{BZ} = \pi/a = 0.39 \times 10^5$ rad/cm).

Sample 3: chains of dots having lateral dimensions of 1025×450 nm^2 placed side by side along the major axis with an edge-to-edge distance $\Delta = 50$ nm (periodicity $a = 500$ nm, 1BZ boundary $q_{BZ} = \pi/a = 0.63 \times 10^5$ rad/cm).

Sample 4: chains of dots having lateral dimensions of 1025×450 nm^2 placed side by side along the minor axis with an edge-to-edge distance $\Delta = 85$ nm (periodicity $a = 1110$ nm, 1BZ boundary $q_{BZ} = \pi/a = 0.28 \times 10^5$ rad/cm).

In all samples the interchain distance is 0.5 μm so that the dipolar magnetic interaction between adjacent chains is negligible.

Brillouin light scattering (BLS) spectra were measured at room temperature by using a 220-mW p-polarized monochromatic light from a solid-state laser of wavelength $\lambda = 532$ nm. Incident light was focused onto the sample surface by means of a camera objective of focal length 50 mm and f number 2. The spot size is about 30 μm in diameter so that several hundreds of nanodots were illuminated at the same time and the information was averaged over such a large number of elements. After a cross-polarization analysis of the backscattered light, a (3 + 3) tandem Fabry-Pérot interferometer was used.[19] In all the experiments the dc magnetic field was parallel to the sample plane and was always directed perpendicularly to the chain's length. For the two series of samples studied here, this direction corresponds either to the easy or to the hard axis of the rectangular elements. The in-plane transferred wave vector $\boldsymbol{q}$ (Bloch wave vector) was perpendicular to $\mathbf{H}$ (Voigt geometry) and parallel to the chain's length. In particular, for samples 1 and 3 [Figs. 1(a) and 1(c), respectively] an external field $\mathbf{H}$ of magnitude $H = 1$ kOe, directed along the y axis (easy axis), was applied. Instead, for samples 2 and 4 [Figs. 1(b) and 1(d), respectively] an external field $\mathbf{H}$ of magnitude $H = 1.5$ kOe was applied along the x axis (hard axis). Measurements were performed in the backscattering geometry, where the magnitude of $\boldsymbol{q}$ is expressed in terms of the light incidence angle (θ) by the relation $q = (4\pi/\lambda)\sin\theta$.

III. THEORETICAL APPROACH FOR NORMAL MODES AND CROSS SECTION

In this section we briefly describe the framework used to obtain the magnonic bands. The method is based on the micromagnetic model, developed by Giovannini *et al.*[16] for periodic magnetic systems. It is an extension of the DMM, originally introduced for calculating the normal modes of single magnetic elements.[14]

We assumed that the dynamic magnetization $\boldsymbol{\delta m}(\boldsymbol{r})$, solution of the linearized equation of motion in a periodic system, has the form of a Bloch wave, viz.

$$\boldsymbol{\delta m}(\boldsymbol{r}) = \boldsymbol{\delta \tilde{m}}(\boldsymbol{r}) e^{i\boldsymbol{q}\cdot\boldsymbol{r}}, \tag{1}$$

where the function $\boldsymbol{\delta \tilde{m}}(\boldsymbol{r})$ has the artificial periodicity of the magnonic crystal, i.e., $\boldsymbol{\delta \tilde{m}}(\boldsymbol{r} + \boldsymbol{R}) = \boldsymbol{\delta \tilde{m}}(\boldsymbol{r})$, and $e^{i\boldsymbol{q}\cdot\boldsymbol{r}}$ is a plane wave with $\boldsymbol{q}$ the Bloch vector and $\boldsymbol{r}$ the in-plane vector. $\boldsymbol{R}$ is the Bravais lattice vector that gives the periodicity of the magnonic crystal. Magnonic modes can thus be seen as propagating waves modulated by the arrays. In particular, for the 2D case the Bravais lattice vector takes the generic form $\boldsymbol{R} = n_1\boldsymbol{a}_1 + n_2\boldsymbol{a}_2$ with $\boldsymbol{a}_1$ and $\boldsymbol{a}_2$ primitive vectors, $0 \leqslant n_i < N_i$ with $i = 1,2$, N_i the number of cells along the $\boldsymbol{a}_i$ direction and $N = N_1\, N_2$.

In our calculations, each dot was divided into cells (parallelepipeds) having size $\Delta_x \times \Delta_y \times \Delta_z = 5$ nm $\times 5$ nm $\times 40$ nm and the ground state was obtained by using a micromagnetic code. The magnetization was assumed to be uniform in each cell and to precess around its equilibrium direction described by the direction of the effective field $\mathbf{H}_{\text{eff}}$. Contributions arising from external (Zeeman), demagnetizing and exchange fields were included in $\mathbf{H}_{\text{eff}}$. The following magnetic parameters obtained from the fit to the BLS frequencies of the Damon-Eshbach mode in the 40-nm-thick continuous Permalloy film were used: saturation magnetization $4\pi M_s = 9$ kG, $\gamma/2\pi = 2.94$ GHz/kOe, and $A = 1.1 \times 10^{-6}$ erg/cm with A the exchange stiffness constant. The large applied magnetic field allowed us to assume that the magnetic ground state was the same for all the dots of a chain.

We have found that, for samples 1 and 2 [Figs. 1(a) and 1(b)], the ground state was a S state, with small deviations from the direction of $\mathbf{H}$ close to the borders. Instead, the calculated ground state for samples 3 and 4 depends on the applied field direction configuration. For the case of dots put side by side along their major axis [Fig. 1(c)] and $\mathbf{H}$ placed along the y axis (major axis), the calculated ground state was a symmetric quasiuniform state where the static magnetization deviates from the collinear configuration because of the dot rounded corners (a sort of onion state). When dots are placed side by side along their minor axis [Fig. 1(d)] and $\mathbf{H}$ is placed along the x axis (minor axis), the calculated ground state was a S state.

Since the interdot dipolar magnetic interaction is relatively weak, the collective modes propagating in magnetic chains can be classified by using the same nomenclature introduced for a single dot of arbitrary shape with in-plane magnetization.[20] The collective mode mainly localized in the center of each element and without nodes is the fundamental (F) mode of the spectrum. Damon-Eshbach-like (nDE) modes are excitations with nodal planes $n = 1, 2, \ldots$ parallel to the local direction of the static magnetization $\mathbf{M}$, while nodal planes perpendicular to the local direction of $\mathbf{M}$ are typical of backwardlike (nBA) modes with $n = 1, 2, \ldots$. Finally, the end modes (nEM) are localized at the edges of each element in the direction of the magnetization (either along the x or y direction) with possible nodal planes of the DE type, viz. parallel to the local direction of $\mathbf{M}$ ($n = 0, 1, 2, \ldots$). Mixed modes, with both parallel and perpendicular nodal planes, are also present but not experimentally detected.

It is useful to give the expression of the differential scattering cross section used to interpret our micromagnetic results (see Sec. IV). Indeed, the evaluation of the differential cross section allows us to assign unambiguously to a given spin-wave mode a given BLS peak. As shown in the Appendix, the differential scattering cross section associated to each magnonic mode of the spectrum turns out to be proportional to the square modulus of the amplitude of the scattered field, viz. $\tilde{\boldsymbol{E}}_{\text{scatt}}$, and takes thus the form

$$\left(\frac{d^2\sigma}{d\Omega\, d\omega}\right)_{p\to s} = C\, N(|\omega' - \omega|)\, \frac{\left|\left(\sum_{\boldsymbol{R}=\boldsymbol{R}_1}^{\boldsymbol{R}_N} e^{i(\Delta\boldsymbol{k}+\boldsymbol{q})\cdot\boldsymbol{R}}\right)\int_{\text{cell}} e^{i\Delta\boldsymbol{k}\cdot\boldsymbol{r}} A(\boldsymbol{r})\, d\boldsymbol{r}\right|^2}{|\tilde{\boldsymbol{E}}_0|^2}\delta(\Omega - |\omega' - \omega|), \tag{2}$$

where σ is the scattering cross section, $d\Omega$ is the differential solid angle, and the subscripts p and s refer to the p and s polarization of the incident and scattered light, respectively. C is a constant depending on geometric and optical parameters, $N(|\omega' - \omega|)$ is the Bose-Einstein thermal factor with ω' and ω the angular frequency of the scattered and incident light, respectively, the sum $\sum_{\boldsymbol{R}=\boldsymbol{R}_1}^{\boldsymbol{R}_N} e^{i(\Delta k+q)\cdot\boldsymbol{R}}$ is performed over N illuminated cells, $\tilde{\boldsymbol{E}}_0$ is the amplitude of the incident electric field, $\Delta k_\alpha = k_\alpha - k'_\alpha$, $\delta(\Omega - |\omega' - \omega|)$ is the Dirac delta, and Ω is the angular frequency of the given collective mode. Here k'_α (k_α) is the α component ($\alpha = x, y$) of the scattered (incident) wave vector projected on the surface and $A(\boldsymbol{r})$ is a quantity depending on the dynamic magnetization and optical properties of the media. In the numerical calculations we have determined the differential scattering cross section associated to each collective mode at a given frequency and for a given Bloch wave vector, because we have adopted in Eq. (2) the selection rule $\Delta \boldsymbol{k} = -\boldsymbol{q}$, which holds rigorously only when the area illuminated by light is infinite.

Calculations of the BLS intensities of collective spin-wave modes in interacting stripes were recently performed.[21] However, these calculations were based on a formalism different from that reported here, consisting of a modification of the fluctuation-dissipation theorem applied to periodic systems and focusing on the stochastic aspect of the scattering problem.

IV. RESULTS AND DISCUSSION

A. Comparison between experimental results and DMM calculations

Representative BLS spectra recorded at the center ($q = 0$) and at the border ($q = \pi/a$) of the 1BZ are shown in Fig. 2 for samples 2 and 3.

The spectra of all samples show several peaks in the frequency range between 3 and 15 GHz. The measured spectra of samples 2 and 4, with **H** applied along the hard axis of the rectangular dots, have a larger number of peaks with respect to those relative to samples 1 and 3. From comparison between the experimental spectra and the calculated mode frequencies and profiles, we could label the detected modes. An appreciable experimental frequency dispersion for the F mode has been found for all the specimens with the exception of that relative to sample 4.

Concerning the BLS intensities of the modes, all the samples exhibit the same trend. In particular, at the center of the 1BZ ($q = 0$) the F mode is the dominant peak. The 1DE mode is also detected, because of the nonvanishing collection angle (about 30°) of the camera objective due to the finite aperture. On increasing the magnitude of $\boldsymbol{q}$, the intensity of the F mode decreases, while the 1DE mode becomes more and more intense. Eventually, in the second Brillouin zone (2BZ) the 1DE mode has the largest intensity (not shown in Fig. 2).

It is well known that in the isolated dot the calculated BLS differential cross section is proportional to the average value of the dynamic magnetization associated to the given spin-wave mode. Hence the F mode (with no nodal planes)

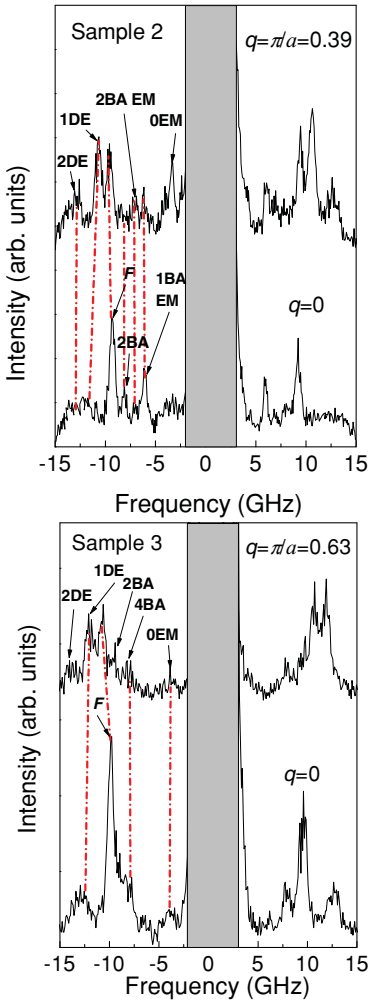

FIG. 2. (Color online) BLS spectra measured at the center and at the border of the 1BZ for samples 2 (top panel) and 3 (bottom panel). The value of q is in units of 10^5 rad/cm. For sample 2 a magnetic field of magnitude $H = 1.5$ kOe was applied along the hard axis of the dots, while for sample 3 a magnetic field of magnitude $H = 1$ kOe was applied along the easy axis of the dots.

exhibits often the largest cross section, but also nBA and nDE modes with an even and low number of nodal planes have a non-negligible scattering cross section (e.g., 2BA, 4BA, and 2DE modes). Moreover, due to the symmetry rules related to coupling with light, the BLS differential cross section can be appreciable also for nDE modes with an odd number of nodal planes like, e.g., for the 1DE mode. Similar conclusions can be drawn also in periodic systems like chains even though also the dependence of the scattering cross section on the Bloch wave vector must be taken into account. The above arguments are in agreement with the experimental observation of the most important BLS active collective modes shown in Fig. 2.

In Fig. 3 the measured and the calculated frequencies are reported for both the 1BZ and the 2BZ for all samples. The overall agreement between the experimental and simulated frequencies for all samples is very good. The only exception is represented by the 1DE mode whose calculated frequencies are in general larger with respect to the experimental ones with

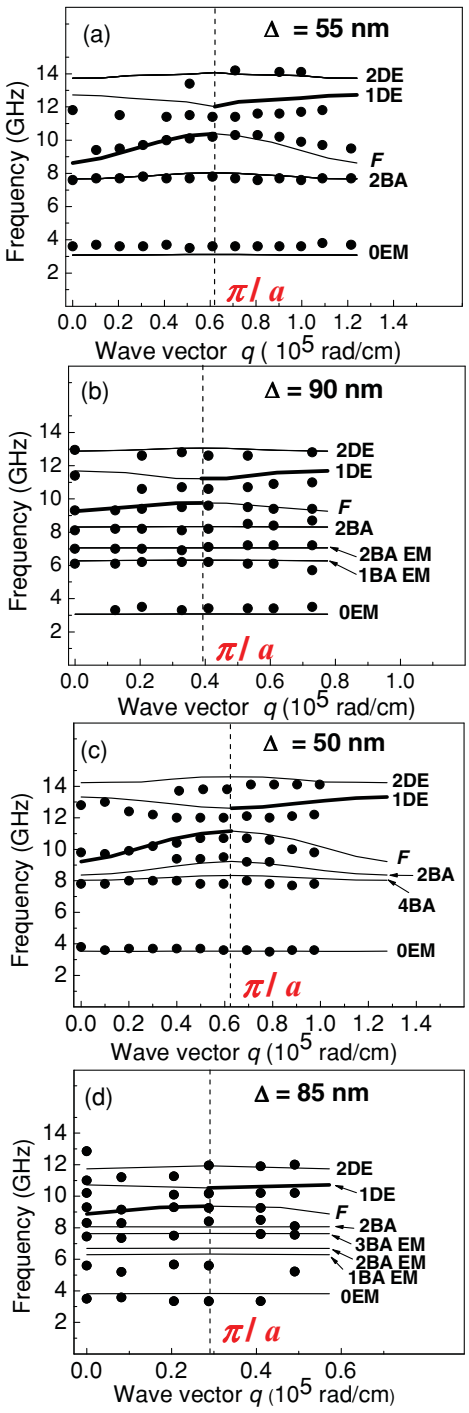

FIG. 3. (Color online) Spin-wave frequency dispersion in the 1BZ and 2BZ. (a) Sample 1; (b) sample 2; (c) sample 3; (d) sample 4, where circles represent BLS data, full lines represent calculated frequencies. The vertical dashed lines indicate the edge of the 1BZ corresponding to q_{BZ} where (a) $q_{BZ} = 0.62 \times 10^5$ rad/cm, (b) $q_{BZ} = 0.39 \times 10^5$ rad/cm, (c) $q_{BZ} = 0.63 \times 10^5$ rad/cm, and (d) $q_{BZ} = 0.28 \times 10^5$ rad/cm. The bold lines mark the calculated collective mode with the largest spectral line in the 1BZ and 2BZ, respectively.

a difference that is at most of about 1 GHz. This could be due to enhanced pinning effects in turn related to an overestimation of the dynamic dipolar magnetic interaction in border regions where the reproduction of the dot curvature by squared cells is inaccurate. Some discrepancies are also present for the 0EM. In fact, as it has been pointed out also by other groups[22] groups, the frequency of the 0EM depends critically on the detailed shape of the dot ends where the modes are localized, so their frequencies are intrinsically difficult to be satisfactorily reproduced with any finite-difference micromagnetic method.

The bold portion of the calculated curves denotes the most intense peak obtained in the calculations by using Eq. (2). It can be seen that the spectral line associated to the F mode is prevalent in the 1BZ, while in the 2BZ the prevalent spectral line belongs to the 1DE mode, confirming the BLS experimental observation according to which the intensity of the F (1DE) peak is larger in the 1BZ (2BZ). These are special cases of the general rule according to which the BLS selects the mode whose effective wavelength matches $2\pi/\Delta k$. Therefore the calculated intensity of the F mode in the 1BZ decreases with q and at the 1BZ boundary it is nearly equal to that of the 1DE. Indeed, due to the light dephasing effect of the exponential $e^{i\Delta \mathbf{k}\cdot\mathbf{r}}$, the 1DE mode has an appreciable differential scattering cross section for $q \neq 0$.

We notice that the BLS experimental frequency dispersion (amplitude of the magnonic band) is more pronounced for the F mode (about 1 GHz in samples 1 and 3, and about 0.5 GHz in sample 2). This is due to the fact that the F mode is the only one which creates a significant stray magnetic field outside of the magnetic element itself. The BLS bandwidths are well predicted by the theoretical calculations and indicate that the dynamic dipolar magnetic interaction is larger in the samples with smaller periodicity, and in particular is more effective in samples 1 and 3, which are put side by side along the major axis.

Our results (both theoretical and experimental) show that the band of the F mode has a minimum at $q = 0$. This can be qualitatively understood taking into account that, for this mode and for $q = 0$, the spin precession along the chain in neighboring dots is in phase, therefore implying a minimum frequency. Instead, the behavior of the dispersion of the 1DE mode is reversed, namely the minimum occurs at the border of the 1BZ ($q_{BZ} = \pi/a$). This behavior deserves a deeper investigation, which will be faced later in more general terms.

On the other side, bandwidths of spin-wave modes belonging to the lowest part of the spectra are very narrow with slight differences depending on the mode considered and on the geometry. The narrow bands of the nBA modes ($n = 2,4$) are due to the fact that the BLS measurements have been performed in the Voigt geometry, i.e., with $\boldsymbol{q}$ perpendicular to $\mathbf{H}$. Furthermore, the bands associated to the 0EM are almost flat essentially because the regions of localization of these modes are small, so that the dynamic dipolar magnetic coupling is weak.

Information about the group velocity of collective modes can be drawn from the analysis of their dispersion. The F mode has the largest group velocity close to the center of the 1BZ ($q = 0$), which we estimated from the calculated dispersion to be nearly 2.17×10^3 m/s and 2.26×10^3 m/s for samples 1 and 3 [panels (a) and (c)], respectively. These group velocities are considerably smaller than the group velocity of the DE mode calculated in the unpatterned continuous film ($v_g = 3.15 \times 10^3$ m/s) whose group velocity represents the upper limit for the dispersion slope of collective excitations in

a 2D periodic structure. On the contrary, the group velocities of spin modes belonging to the low-frequency part of BLS spectra are very small.

If one looks in more detail at the calculated magnonic bands in the 1BZ, a different behavior characterizes the bands belonging to nBA and nDE modes, respectively with $n = 1, 2, \ldots$. Indeed, while the frequencies of nBA modes at $q_{BZ} = \pi/a$ are always higher than the corresponding ones at $q = 0$ independently of the number of nodes, for nDE modes the situation is more complex. In particular, for an odd number of nodes, frequencies at $q_{BZ} = \pi/a$ are lower than the ones at $q = 0$, while the frequency behavior is reversed when the number of nodes is even. For both families of modes, the bandwidth decreases with increasing the number of nodes.

Interestingly, additional magnonic bands in the lowest part of the spectrum were observed for samples 2 and 4, where the rectangular elements are put side by side along their minor axis. We have found, by inspection of the mode profiles and from scattering cross-section calculations, that these bands can be assigned to nBA EM with $n = 1,2,3 \ldots$, i.e., to a sort of hybrid between conventional EM and nBA modes. The modes are assigned by counting the number of nodal planes that are found in only one half of the element. As a matter of fact, in large dots, the lateral wells of the internal field are rather deep allowing also the presence of these laterally localized modes of BA type.

The nature of these modes is illustrated in Fig. 4. They have nodal planes of BA type perpendicular to the local static magnetization close to the dot edges and are symmetric under inversion with respect to the center of the dot. As for the 0EM band, the flatness of the corresponding bands is due to the weak dynamic dipolar magnetic coupling. In general, the calculated scattering intensity from these modes is weak (with the exception of the 1BA EM which has a high intensity) and is mainly due to the S state. Moreover, it is not easy to identify them in the spectra.

As a general comment on the obtained results, we remark that samples 1 and 3, where dots are put side by side along the major axis, are characterized by the largest frequency oscillation amplitude of the mode frequencies (magnonic bands), especially for the F mode. In fact, even if the dots of the four samples were arranged in two different configurations, in samples 1 and 3 modes are much more efficiently dipolarly coupled with respect to those of samples 2 and 4, because of the smaller periodicity and the larger facing regions between adjacent dots. Note that the presence of magnonic bands with significant amplitude corresponds to propagation of collective modes with nonvanishing group velocity: This is an important requirement to overcome the large spin-wave damping in spin-logic devices based on metallic ferromagnets and spin-wave waveguides.[23]

B. Discussion about the interdot magnetic coupling and its dependence on separation

In this subsection we investigate, by means of micromagnetic calculations, the effect of interdot dipolar magnetic coupling on mode dispersions as a function of interdot separation. In order to estimate the dependence of frequency gaps on the interdot coupling, in Fig. 5 we plot the mode frequency as a function of interdot separation.

The analysis was carried out for all the four series of samples, obtaining similar results. We therefore illustrate here in detail the results corresponding to the configuration represented by sample 1, but for different interdot separations. Full lines (black) denote frequencies of magnonic modes for

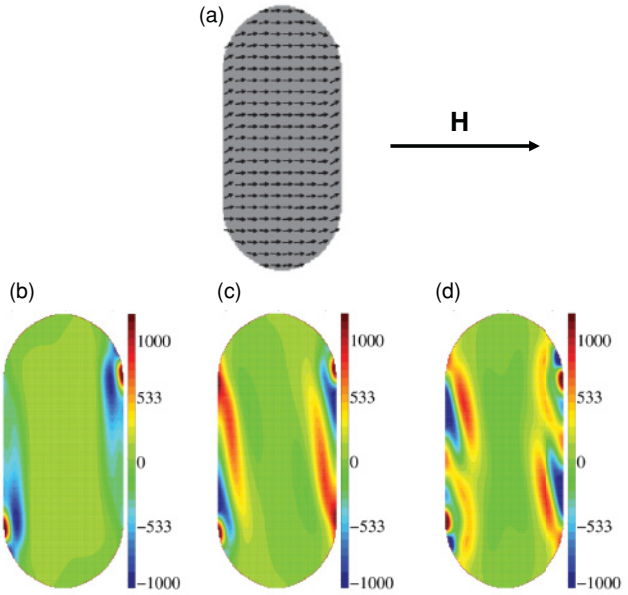

FIG. 4. (Color online) (a) Calculated static magnetization distribution for the dot under an external field $H = 1.5$ kOe. The direction of the applied magnetic field **H** is also shown. Calculated real part of $\delta m_z(\boldsymbol{r})$ for the nBA EM corresponding to configuration shown in Fig. 1(d) and at $q = 0$: (b) 1BA EM, (c) 2BA EM, (d) 3BA EM.

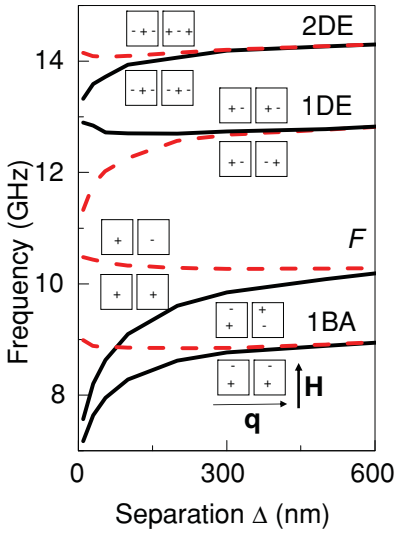

FIG. 5. (Color online) Calculated frequency behavior vs interdot separation for sample 1. Full lines (black): frequencies at $q = 0$. Dashed lines (red): frequencies at $q_{BZ} = \pi/a$. In the insets, the sign of the dynamic magnetization of the magnonic modes is represented by means of the symbols "+" and "−" for a given mode in two neighboring dots. Each dot is pictorially schematized as a rectangle.

$q = 0$, while the frequency curves corresponding to $q_{BZ} = \pi/a$ are indicated by dashed lines (red). These lines mark the upper and lower limits of each allowed magnonic band.[16] We remind that the frequency gaps between the shown spin-wave modes can be occupied by calculated mixed modes which are not observed in the experimental spectra.

As expected, for large interdot separation where coupling is negligible, each mode is characterized by a single frequency value corresponding to the spectrum of stationary modes of a single magnetic element and whose value is independent of $\boldsymbol{q}$. On decreasing the separation, interdot coupling gives rise to the appearance of bands. Within each band the frequency of the collective modes depends on $\boldsymbol{q}$. This is in turn related to the effect of dynamic dipolar (stray) magnetic field associated with each collective mode which is enhanced at small Δ. A similar behavior characterizes also the experimental frequencies as a function of separation (not shown). We do not show the low-frequency modes, because the corresponding bands are flat even at small separation. For all the studied configurations, independent of the direction of the applied field (either along the x or y axis), the largest bandwidth is that of the F mode. This behavior is not surprising, because the F mode has the largest stray field at any separation, as found in interacting magnetic nanostripes.[7] Moreover, the bandwidth at small separation is more pronounced for collective modes corresponding to the configurations where rectangular elements were put side by side along their major axis. The larger bandwidth is related to the smaller periodicity a which in turn leads to larger stray fields at a fixed separation with respect to lines of dots placed side by side along their minor axis. On the other hand, one sees that the frequency curves of a given collective mode at $q = 0$ and at $q_{BZ} = \pi/a$ tend to merge asymptotically when the separation exceeds a few hundreds of nm, corresponding to the spectrum of stationary modes of a single magnetic element.

Interestingly, in Fig. 5 one notes a superposition of the F mode frequency curves with those of 1BA mode at small separation. Such a band superposition is related to the large bandwidth of the F mode occurring when dots are put side by side along the major axis of the rectangular element. For samples 2 and 4, where the dots are put side by side along the minor axis, this superposition does not occur anymore.

Another significant feature, common to all the configurations, is the narrowing of the frequency gaps, as $\Delta \to 0$, either at $q = 0$ or at $q_{BZ} = \pi/a$. In particular, the frequency gap between the F mode and the 1DE mode is smaller for $q_{BZ} = \pi/a$, while that between the 1DE and 2DE modes is smaller for $q = 0$. As a matter of fact, for small separation the energetic cost required to excite the F mode at $q_{BZ} = \pi/a$, namely in the antiphase configuration, is almost the same as that of the 1DE mode. The difference is represented by the frequency gap between the two modes at the 1BZ boundary. Similar considerations can be carried out to understand the narrowing of the frequency gap at $q = 0$ between the 1DE and 2DE modes as $\Delta \to 0$.

Finally, it is interesting to shortly discuss why for some modes (2DE, F, 1BA) the red curve is at higher frequency with respect to the black one, while for the 1DE mode the opposite situation occurs. To this respect, we have found that, in general, the behavior of the frequency of the F, nDE, and nBA collective modes versus q in the Voigt geometry can be described in terms of a simple rule, illustrated by the insets of Fig. 5. The rule states that when modes in neighboring dots couple to each other with the same phase on the facing sides of each pair of dots, the excitation frequency is lower with respect to the case when modes in neighboring dots couple to each other with opposite phase. A similar explanation of the frequency behavior, but restricted to high-frequency modes only (corresponding to the F and nDE modes of this system), was recently formulated for a 1D array of dipolarly interacting stripes[9] in terms of coupling of dynamic dipolar magnetic fields in neighboring elements.

The stated rule can also be derived from the study of the frequency behavior as a function of the wave vector in a film and from the conclusions of previous studies on "optical" and "acoustical" spin waves in antiferromagnetically coupled multilayers (see, e.g., Ref. 24). Looking at the insets of Fig. 5, one can easily see that the above-mentioned rule is verified. It is interesting to note that the behavior of the frequency curves of the F mode at $q = 0$ and at $q_{BZ} = \pi/a$ is very similar to that found by Kostilev *et al.*[25] for the corresponding collective mode in a 1D array of stripes as a function of the interstripe separation by means of an analytical model.

The reason for the rule is that optical-like modes force the dynamic magnetization of the whole chain of interacting dots to gain more nodes of DE character with respect to the corresponding acoustical-like modes. In this case, the optical-like modes have a larger effective wave vector and therefore a larger angular frequency, because Ω is a monotonic increasing function of the wave vector.

Interestingly, if one considers the ideal case of rectangular elements, the dispersion of the resonant mode of an in-plane magnetized stripe can be found as $\Delta \to 0$. In order to obtain it, one should, however, include in the micromagnetic calculation the exchange interaction between neighboring dots, which we have not considered here.

V. CONCLUSIONS

In this paper the behavior of collective spin modes in 1D magnetic arrays of rectangular dots was investigated. The study was carried out by using a micromagnetic model based upon the DMM, generalized to dots interacting via both static and dynamic dipolar magnetic coupling. Magnonic bands were studied for a series of different geometries to evaluate the effect of dipolar magnetic coupling on spin-wave mode frequencies. Results of the micromagnetic calculations compared well with available BLS measurements for the whole set of configurations studied. In addition to the usual spin-wave modes (0EM, nBA, and nDE), we have found a set of nBA EM ($n = 1,2,3$) confirming the experimental observations. The main finding was the presence of magnonic bands independently of the studied configuration, especially for the F and the 1DE mode, that can be considered as spin-wave modes with a strong collective nature. A simple rule able to explain the band opening passing from the center to the edge of the 1BZ for the Voigt geometry was proposed. This band rule was formulated in terms of coupling of collective mode phases in neighboring dots and is independent of the configuration investigated in this study. The general validity of the band rule lies in its applicability to the band behavior of

each family of collective modes studied here, namely nDE and nBA, and can explain also the band behavior of mixed modes and nEM.

Micromagnetic calculations allowed us also to investigate the behavior of collective spin-wave modes as a function of separation Δ. We found a widening of bandwidths for all the collective modes with decreasing Δ together with a narrowing of frequency gaps either at $q=0$ or at $q_{BZ}=\pi/a$ depending on the collective mode studied. For all the analyzed configurations the effect of interdot coupling can be considered non-negligible up to $\Delta \approx 700$ nm for the F mode and up to $\Delta \approx 300$ nm for other modes (nBA and nDE). For separations larger than 700 nm the corresponding magnonic bands become flat and the spin-wave mode frequencies tend to those of an isolated magnetic element.

Prediction of amplitude of modes frequency oscillation (magnonic band) for a vanishing separation represents an important property to identify the behavior of a one-dimensional magnonic meta-material and it is preliminary to any desired application of magnonic crystal for realization of spin logic devices, filters and waveguides operating in the GHz frequency range. From this point of view our chains can be considered as an example of quasi-continuous one-dimensional meta-materials.

ACKNOWLEDGMENTS

The research leading to these results has received funding from the European Community's Seventh Framework Programme (FP7/2007-2013) under Grant Agreement No. 228673 (MAGNONICS) and National Research Foundation (NRF), Singapore under Grant No. NRFG-CRP 2007-05. Consorzio Nazionale Interuniversitario per le Scienze Fisiche della Materia (CNISM) support is also acknowledged. The authors thank N. Singh and S. Goolaup for experimental support.

APPENDIX

In this Appendix we present the derivation of the differential scattering cross-section formula for interacting magnetic elements. Following the formalism developed for the continuous film[26] and for the single magnetic element, the calculation of the scattering cross section in two-dimensional arrays of interacting dots requires first to express the amplitude of the scattered electric field. The wave propagation equation in a magnetic medium with perturbed dielectric constant expanded to the first order reads

$$\nabla \times \nabla \times \boldsymbol{E}_{\text{scatt}} + \frac{1}{c^2}\varepsilon_0 \frac{\partial^2}{\partial t^2}\boldsymbol{E}_{\text{scatt}} = -\frac{1}{c^2}\overleftrightarrow{\delta\varepsilon}\,\frac{\partial^2}{\partial t^2}\boldsymbol{E}_0, \quad \text{(A1)}$$

where ε_0 is the dielectric constant of the unperturbed mean or relative permeability, $\overleftrightarrow{\delta\varepsilon}$ is the tensor representing the fluctuation of the polarization, $\boldsymbol{E}_0(x,y,z,t) = \tilde{\boldsymbol{E}}_0(z)e^{i(k_x x + k_y y + \omega t)}$ is the p-polarized incident field (zero order) with $\tilde{\boldsymbol{E}}_0$ the incident field amplitude, $\boldsymbol{E}_{\text{scatt}}(x,y,z,t) = \tilde{\boldsymbol{E}}_{\text{scatt}}(z)e^{i(k'_x x + k'_y y + \omega' t)}$ is the scattered field (first order) with $\tilde{\boldsymbol{E}}_{\text{scatt}}$ the scattered field amplitude, and $\boldsymbol{k}_\parallel$ ($\boldsymbol{k}'_\parallel$) is the incident (scattered) light wave vector; in particular, $k_\parallel = (2\pi/\lambda)\sin\theta$ ($k'_\parallel = (2\pi/\lambda)\sin\theta'$) is the in-plane incident (scattered) wave vector component with $\theta(\theta')$ the corresponding incidence (scattered) angle; $\omega(\omega')$ is the angular frequency of the incident (scattered) light, and c is the speed of light. By introducing the Fourier transform of $\boldsymbol{E}_{\text{scatt}}$ with respect to x, y, z, and t, the Fourier transform of Eq. (A1) can be written in terms of the electric field (incident and scattered) amplitudes, namely

$$\left(k'^2_\parallel - \frac{\partial^2}{\partial z^2}\right)\tilde{\boldsymbol{E}}_{\text{scatt}} - \frac{\omega'^2}{c^2}\varepsilon_0\,\tilde{\boldsymbol{E}}_{\text{scatt}} = -\frac{\omega^2}{(2\pi)^{3/2}c^2}\int \overleftrightarrow{\delta\varepsilon}\,\tilde{\boldsymbol{E}}_0\, e^{i(\Delta k_x x + \Delta k_y y)} e^{i(\omega-\omega')t}\,dx\,dy\,dt, \quad \text{(A2)}$$

with $\Delta k_\alpha = k_\alpha - k'_\alpha$ ($\alpha = x,y$). In particular, the components of the light incident wave vector are $k_x = k_\parallel \cos\phi$, $k_y = k_\parallel \sin\phi$ where ϕ is the azimuthal angle of light, viz. the angle between the incidence plane and the x-z plane. Analogously, the corresponding components of the scattered wave vector read $k'_x = k'_\parallel \cos\phi$ and $k'_y = k'_\parallel \sin\phi$, respectively. Equation (A2) can be solved by introducing the $g(z,z')$ Green's function and by using the Green's-function method. The solution $\tilde{\boldsymbol{E}}_{\text{scatt}}$ can thus be written in the form

$$\tilde{\boldsymbol{E}}_{\text{scatt}}(z) = -\frac{\omega^2}{(2\pi)^{3/2}c^2}\int g(z,z')\,\overleftrightarrow{\delta\varepsilon}(x,y,z',t) \times \tilde{\boldsymbol{E}}_0(z')\,e^{i\Delta\boldsymbol{k}\cdot\boldsymbol{r}} e^{i\Delta\omega t}\,dx\,dy\,dz'\,dt, \quad \text{(A3)}$$

where the Green's function $g(z,z')$ is the same as the one defined for multilayers, whereas $\tilde{\boldsymbol{E}}_0$ is the amplitude of the incident electric field and $\Delta\omega = \omega - \omega'$. Analogously to the case of continuous film, expressing $\overrightarrow{\delta\varepsilon}$ in terms of the dynamic magnetization amplitudes and integrating over z leads to $\tilde{\boldsymbol{E}}_{\text{scatt}} \propto \delta(\Omega - |\omega' - \omega|)\int_{\text{zone}} e^{i\Delta\boldsymbol{k}\cdot\boldsymbol{r}} A(\boldsymbol{r})d\boldsymbol{r}$ where $\boldsymbol{r} = (x,y)$, $\delta(\Omega - |\omega' - \omega|)$ is the Dirac delta, and Ω is the angular frequency of the given collective mode. The integral is extended to the zone illuminated by light. The quantity $A(\boldsymbol{r})$ is in turn expressed as the integral over z of contributions proportional to the polarization. The integral over z contains four terms associated to scattering so that the scattered field refers to four scattering channels including reflection from the back surface of magnetic medium given by (i) reflection-scattering-reflection, (ii) direct scattering, (iii) scattering-reflection, and (iv) reflection-scattering. Each of these terms contains the magneto-optic complex constant K expressing the first-order magneto-optic or Faraday effect and is proportional to the first-order contribution of the dynamic magnetization to the differential scattering cross section. Due to the surface periodicity the integrand $e^{i\Delta\boldsymbol{k}\cdot\boldsymbol{r}}A(\boldsymbol{r})$ appearing in the expression of $\tilde{\boldsymbol{E}}_{\text{scatt}}$ can be written in the particle located in $\boldsymbol{R}$ as $e^{i\Delta\boldsymbol{k}\cdot(\boldsymbol{r}+\boldsymbol{R})}A(\boldsymbol{r}+\boldsymbol{R})$ where $\boldsymbol{r}$ is now restricted to the reference particle ($\boldsymbol{R}=0$). In particular, $e^{i\Delta\boldsymbol{k}\cdot(\boldsymbol{r}+\boldsymbol{R})} = e^{i\Delta\boldsymbol{k}\cdot\boldsymbol{r}}e^{i\Delta\boldsymbol{k}\cdot\boldsymbol{R}}$ and according to the Bloch theorem $A(\boldsymbol{r}+\boldsymbol{R}) = e^{i\boldsymbol{q}\cdot\boldsymbol{R}}A(\boldsymbol{r})$. Taking into account these substitutions and summing over the illuminated N cells, the integral $\int_{\text{zone}}$ expressing $\tilde{E}_{\text{scatt}}$ can be substituted by $\sum_{\boldsymbol{R}=\boldsymbol{R}_1}^{\boldsymbol{R}_N} e^{i(\Delta\boldsymbol{k}+\boldsymbol{q})\cdot\boldsymbol{R}}\int_{\text{cell}}$ yielding

$$\tilde{\boldsymbol{E}}_{\text{scatt}} \propto \delta(\Omega - |\omega' - \omega|)\left(\sum_{\boldsymbol{R}=\boldsymbol{R}_1}^{\boldsymbol{R}_N} e^{i(\Delta\boldsymbol{k}+\boldsymbol{q})\cdot\boldsymbol{R}}\right) \times \int_{\text{cell}} e^{i\Delta\boldsymbol{k}\cdot\boldsymbol{r}}A(\boldsymbol{r})\,d\boldsymbol{r} \propto FS, \quad \text{(A4)}$$

where $F = \sum_{\boldsymbol{R}=\boldsymbol{R}_1}^{\boldsymbol{R}_N} e^{i(\Delta \boldsymbol{k}+\boldsymbol{q})\cdot\boldsymbol{R}}$ is a factor depending on the Bloch wave vector. In particular, $F = F(\theta,\theta',\boldsymbol{q})$ and $S = \int_{\text{cell}} e^{i\Delta\boldsymbol{k}\cdot\boldsymbol{r}} A(\boldsymbol{r})\, d\boldsymbol{r}$ is a term related to the scattered field obtained for the single dot. The quantity $A(\boldsymbol{r})$ is a linear combination of the components of the dynamic magnetization. According to Eq. (A4), the differential scattering cross section is thus proportional to a term depending on the single dot times a factor F whose form depends on the extension of the illuminated area. By considering the ideal case of an infinite illuminated area we get an infinite sum over the cells, namely $\sum_{\boldsymbol{R}} e^{i(\Delta \boldsymbol{k}+\boldsymbol{q})\cdot\boldsymbol{R}} \propto \delta(\Delta\boldsymbol{k}+\boldsymbol{q})$ so that the selection rule $\Delta\boldsymbol{k} = -\boldsymbol{q}$ is rigorously fulfilled. The S term in Eq. (A4) can be seen as an efficiency factor depending on the mode profile and on the Bloch wave vector. The differential scattering cross section of Eq. (2) is finally obtained by performing the square modulus of $\tilde{\boldsymbol{E}}_{\text{scatt}}$.

[1] J. Jorzick, S. O. Demokritov, B. Hillebrands, B. Bartenlian, C. Chappert, D. Decanini, F. Rousseaux, and E. Cambril, Appl. Phys. Lett. **75**, 3859 (1999).

[2] S. Demokritov and B. Hillebrands, in *Spin Dynamics in Confined Magnetic Structures I*, edited by B. Hillebrands and K. Ounadjela, Springer Series in Topics in Applied Physics (Springer-Verlag, Berlin, 2002).

[3] S. Tacchi, M. Madami, G. Gubbiotti, G. Carlotti, H. Tanigawa, T. Ono, and M. P. Kostilev, Phys. Rev. B **82**, 024401 (2010), and references therein.

[4] A. Khitun, M. Bao, and K. L. Wang, IEEE Trans. Magn. **44**, 2141 (2008).

[5] T. Schneider, A. A. Serga, B. Leven, B. Hillebrands, R. L. Stamps, and M. P. Kostylev, Appl. Phys. Lett. **92**, 022505 (2008).

[6] S. Neusser and D. Gründler, Adv. Mater. **21**, 2927 (2009).

[7] G. Gubbiotti, S. Tacchi, G. Carlotti, N. Singh, S. Goolaup, A. O. Adeyeye, and M. Kostylev, Appl. Phys. Lett. **90**, 092503 (2007).

[8] V. V. Kruglyak, S. O. Demokritov, and D. Grundler, J. Phys. D: Appl. Phys. **43**, 264001 (2010).

[9] G. Gubbiotti, S. Tacchi, M. Madami, G. Carlotti, A. O. Adeyeye, and M. Kostylev, J. Phys. D: Appl. Phys. **43**, 264003 (2010).

[10] A. Imre, G. Csaba, L. Ji, A. Orlov, G. H. Bernstein, and W. Porod, Science **311**, 205 (2006); S. Kurtz, E. Varga, M. J. Siddiq, M. Niemier, W. Porod, X. S. Hu, and G. H. Bernstein, J. Phys.: Condens. Matter **23**, 053202 (2011).

[11] G. Gubbiotti, G. Carlotti, P. Vavassori, M. Kostylev, N. Singh, S. Goolaup, and A. O. Adeyeye, Phys. Rev. B **72**, 224413 (2005).

[12] M. Kostylev, P. Schrader, R. L. Stamps, G. Gubbiotti, G. Carlotti, A. O. Adeyeye, S. Goolaup, and N. Singh, Appl. Phys. Lett. **92**, 132504 (2008).

[13] Z. K. Wang, V. L. Zhang, H. S. Lim, S. C. Ng, M. H. Kuok, S. Jain, and A. O. Adeyeye, Appl. Phys. Lett. **94**, 083112 (2009).

[14] M. Grimsditch, L. Giovannini, F. Montoncello, F. Nizzoli, G. K. Leaf, and H. G. Harper, Phys. Rev. B **70**, 054409 (2004).

[15] F. Montoncello, L. Giovannini, F. Nizzoli, H. Tanigawa, T. Ono, G. Gubbiotti, M. Madami, S. Tacchi, and G. Carlotti, Phys. Rev. B **78**, 104421 (2008).

[16] L. Giovannini, F. Montoncello, and F. Nizzoli, Phys. Rev. B **75**, 024416 (2007).

[17] Ki-Suk Lee, Dong-Soo Han, and Sang-Koog Kim, Phys. Rev. Lett. **102**, 127202 (2009).

[18] A. V. Chumak, P. Pirro, A. A. Serga, M. P. Kostylev, R. L. Stamps, H. Schultheiss, K. Vogt, S. J. Hermsdoerfer, B. Laegel, P. A. Beck, and B. Hillebrands, Appl. Phys. Lett. **95**, 262508 (2009).

[19] J. R. Sandercock, in *Light Scattering in Solids III*, Topics in Applied Physics Vol. 51, edited by M. Cardona and G. Güntherodt (Springer, Berlin, 1982), p. 173.

[20] F. Montoncello and F. Nizzoli, in *Magnetic Properties of laterally confined nanometric structures* (Transworld Research Network, 2006), p. 131; G. Gubbiotti, M. Madami, S. Tacchi, A. O. Adeyeye, S. Goolaup, N. Sing and A. N. Slavin, J. Magn. Magn. Mat. **316**, e338 (2007).

[21] M. P. Kostylev and A. A. Stashkevich, Phys. Rev. B **81**, 054418 (2010).

[22] G. Gubbiotti, G. Carlotti, T. Okuno, M. Grimsditch, L. Giovannini, F. Montoncello, and F. Nizzoli, Phys. Rev. B **72**, 184419 (2005); P. S. Keatley, V. V. Kruglyak, A. Neudert, E. A. Galaktionov, R. J. Hicken, J. R. Childress, and J. A. Katine, *ibid.* **78**, 214412 (2008); J. M. Shaw, T. J. Silva, M. L. Schneider, R. D. McMichael, *ibid.* **79**, 184404 (2009).

[23] S. Neusser, G. Duerr, H. G. Bauer, S. Tacchi, M. Madami, G. Woltersdorf, G. Gubbiotti, C. H. Back, and D. Grundler, Phys. Rev. Lett. **105**, 067208 (2010).

[24] R. Zivieri, L. Giovannini, and Nizzoli, Phys. Rev. B **62**, 14950 (2000).

[25] M. P. Kostylev, A. A. Stashkevich, and N. A. Sergeeva, Phys. Rev. B **69**, 064408 (2004).

[26] R. Zivieri, L. Giovannini, and P. Vavassori, in *Magnetic Nanostructures*, ed., H. S. Nalwa (American Scientific, Los Angeles, 2002); L. Giovannini, R. Zivieri, G. Gubbiotti, G. Carlotti, L. Pareti, and G. Turilli, Phys. Rev. B **63**, 104405 (2001), and references therein.